Genetically Engineered Mice for Combinatorial Cardiovascular Optobiology

Frank K. Lee[1], Jane C. Lee[1], Bo Shui[1], Shaun Reining[1], Megan Jibilian[1], David M. Small[2], Jason S. Jones[2], Nathaniel H. Allan-Rahill[2], Michael R.E. Lamont[2], Megan A. Rizzo[3], Sendoa Tajada[4], Manuel F. Navedo[5], Luis Fernando Santana[4], Nozomi Nishimura[2], Michael. I. Kotlikoff[1*]

Department of Biomedical Sciences[1] and Nancy E. and Peter C. Meinig School of Biomedical Engineering[2], Cornell University,

Department of Physiology, University of Maryland School of Medicine[3]

and

Departments of Physiology and Membrane Biology[4], and Pharmacology[5], University of California, Davis School of Medicine

*Corresponding Author: Michael Kotlikoff (mik7@cornell.edu)

300 Day Hall

Cornell University

Ithaca, NY 14853

Abstract

Optogenetic effectors and sensors provide a novel real-time window into complex physiological processes, enabling determination of molecular signaling processes within functioning cellular networks. However, the combination of these optical tools in mice is made practical by construction of genetic lines that are optically compatible and genetically tractable. We present a new toolbox of 21 mouse lines with lineage -specific expression of optogenetic effectors and sensors for direct biallelic combination, avoiding the multiallelic requirement of Cre recombinase -mediated DNA recombination, focusing on models relevant for cardiovascular biology. Optogenetic effectors (11 lines) or Ca^{2+} sensors (10 lines) were selectively expressed in cardiac pacemaker cells, cardiomyocytes, vascular endothelial and smooth muscle cells, alveolar epithelial cells, lymphocytes, glia, and other cell types. Optogenetic effector and sensor function was demonstrated in numerous tissues. Arterial/arteriolar tone was modulated by optical activation of the second messengers $InsP_3$ (optoα1AR) and cAMP (optoß2AR), or Ca^{2+}-permeant membrane channels (CatCh2) in smooth muscle (Acta2) and endothelium (Cdh5). Cardiac activation was separately controlled through activation of nodal/conducting cells or cardiac myocytes. We demonstrate combined effector and sensor function in biallelic mouse crosses: optical cardiac pacing and simultaneous cardiomyocyte Ca^{2+} imaging in $HCN4^{BAC}$-CatCh2/αMHC-GCaMP8 crosses. These experiments highlight the potential of these mice to explore cellular signaling *in vivo*, in complex tissue networks.

Introduction

Optogenetic effectors and sensors enable the interrogation of complex biological signaling networks at the molecular level *in vivo* (Akerboom et al., 2013; Fenno, Yizhar, & Deisseroth, 2011; Gengyo-Ando et al., 2017; Kotlikoff, 2007; Tsien, 2003). The power of these molecular tools is optimized in mammalian systems by genetic lineage specification and combinatorial strategies. The former provides the ability to activate or determine the responses of individual cellular components of a complex network, whereas the latter, using spectrally compatible optogenetic tools, enables the dissection of the network by activation of defined elements and simultaneous interrogation of individual system component responses, thereby significantly enhancing the ability to understand functional networks. Although simple in concept, the usefulness of optogenetic tools in mammalian systems requires a parsimonious allelic strategy that minimizes experimental crosses, while supporting robust and consistent sensor/effector expression. For example, while DNA recombination strategies can achieve lineage specificity by crossbreeding Cre recombinase and floxed responder mouse lines (Zariwala et al., 2012), the attendant allelic requirements render this approach impractical for combinatorial experiments using multiple optogenetic tools. Such experiments are facilitated by the design and assembly of sets of individual mono-allelic lines that strategically place spectrally distinct optogenetic effectors and sensors in interacting cell lineages, allowing simple crosses to probe cell-cell signaling. Here we report a marked expansion of the mammalian optogenetic toolbox through the development of multiple mouse lines designed for combinatorial experiments within the cardiovascular system. Interacting vascular, neural, and muscular tissues are targeted

through a variety of genetic strategies, expression specificity confirmed, and examples of their use provided.

Results

We report the generation of CHROMus (Cornell/National Heart Lung Blood Resource for Optogenetic Mouse Signaling) mice, 21 lines of optogenetic sensor and effector mice, in which the expression of the transgene is lineage specified (Table 1) and demonstrate the utility of these lines for *in vivo* and *ex vivo* imaging. The optogenetic effector proteins we selected for this toolbox were optoα1AR (Airan, Thompson, Fenno, Bernstein, & Deisseroth, 2009), optoß2AR (Airan et al., 2009), and CatCh2 (Zhang, Wang, Boyden, & Deisseroth, 2006) for light activation of $InsP_3$ or cAMP secondary messenger pathways or Ca^{2+} membrane channel, respectively. Each of the open reading frames for the optogenetic proteins were linked to an IRES element and bacterial LacZ ORF for simple screening. The fluorescent GECI proteins, GCaMP and RCaMP, in reporter lines were derived from circularly permutated EGFP and RFP constructs for *in vivo*, real-time reporting of cellular Ca^{2+} signaling (Table 1 – figure supplement 1).

CHROMus mice can be used directly as individual optogenetic effector or fluorescent reporter lines to study real-time response to light activation of the target tissue or to study cellular or subcellular Ca^{2+} signaling in response to various physiological stimuli. However, the system provides the novel opportunity to create novel effector/reporter mouse combinations to study the complex network of physiological signals and

Table 1. List of BACs and PCR primers for CHROMus mice.

CHROMus™ ID	Transgenic Line	Tissue/Sensor Type (**E**ffector or **S**ensor)	Promoter or BAC	genotyping primer 1	genotyping primer 2
B3	Acta2^{BAC}-RCaMP1.07	Smooth muscle-S	RP23-370F21	GCTTGTCTGTAAGCGGATGCC	TGCTGCTGCCACTCTAGTGAGAAA
B4	αMHC-GCaMP8	Cardiac muscle-S	Addgene 55594	AAGGGCGAGGAGCTGTTCA	CGATCTGCTCTTCAGTCAGTTGGT
B5	αMHC-CatCh2_IRES_lacZ	Cardiac muscle-E	Addgene 55594	GGAGATCTATGTGTGCGCTATC	CCAGCAGTTCTTCGACATCA
B6	Acta2^{BAC}-Optoα1AR_IRES_lacZ	Smooth muscle-E	RP23-370F21	GGGTTGGTCCCGCTATATTC	GAAGGCAGGGATGGTCATAAA
B7	Acta2^{BAC}-Optoß2AR_IRES_lacZ	Smooth muscle-E	RP23-370F21	ATAGCTCTCAGCAACCTGTTGGGT	TTCAACACGGTTTGGAGGCG
B8	Acta2^{BAC}-CatCh2_IRES_lacZ	Smooth muscle-E	RP23-370F21	GGAGATCTATGTGTGCGCTATC	CCAGCAGTTCTTCGACATCA
B10	HCN4^{BAC}-GCaMP8	Cardiac conduction-S	RP23-281H22	AAGGGCGAGGAGCTGTTCA	CGATCTGCTCTTCAGTCAGTTGGT
B14	Acta2^{BAC}-GCaMP5_mCherry	Smooth muscle-S	RP23-370F21	AAGGGCGAGGAGCTGTTCA	CGATCTGCTCTTCAGTCAGTTGGT
B15	Cx40^{BAC}-GCaMP5_mCherry	Endothelium-S	RP24-255O4	AAGGGCGAGGAGCTGTTCA	CGATCTGCTCTTCAGTCAGTTGGT
B16	Dbh^{BAC}-CatCh2_IRES_lacZ	Sympathetic-E	RP23-354N13	GGAGATCTATGTGTGCGCTATC	CCAGCAGTTCTTCGACATCA
B17	HCN4^{BAC}-CatCh2_IRES_lacZ	Cardiac conduction-E	RP23-281H22	GGAGATCTATGTGTGCGCTATC	CCAGCAGTTCTTCGACATCA
B19	Acta2^{BAC}-GCaMP2	Smooth muscle-S	RP23-370F21	AAGGGCGAGGAGCTGTTCA	CGATCTGCTCTTCAGTCAGTTGGT
B20	Cdh5^{BAC}-GCaMP8	Endothelium-S	RP23-453P1	AAGGGCGAGGAGCTGTTCA	CGATCTGCTCTTCAGTCAGTTGGT
B22	Lck ^{BAC}-Optoα1AR_IRES_lacZ	T cells-E	RP24-159E19	GGGTTGGTCCCGCTATATTC	GAAGGCAGGGATGGTCATAAA
B23	SP-C ^{BAC}-GCaMP8	Alveolar-S	RP23-247J9	AAGGGCGAGGAGCTGTTCA	CGATCTGCTCTTCAGTCAGTTGGT
B26	Cdh5^{BAC}-Optoα1AR_IRES_lacZ	Endothelium-E	RP23-453P1	GGGTTGGTCCCGCTATATTC	GAAGGCAGGGATGGTCATAAA
B27	Cdh5^{BAC}-Optoß2AR_IRES_lacZ	Endothelium-E	RP23-453P1	AACCTTGGAGGCTGGAAAGTAG	TTCAACACGGTTTGGAGGCG
B28	Cdh5^{BAC}-CatCh2_IRES_lacZ	Endothelium-E	RP23-453P1	GGAGATCTATGTGTGCGCTATC	CCAGCAGTTCTTCGACATCA
B34	Acta2^{BAC}-GCaMP8.1_mVermilion	Smooth muscle-S	RP23-370F21	AAGGGAGAGGAGCTGTTCA	CGATCTGCTCCTCTGTCAGCTGGT
B35	FoxJ1^{BAC}-GCaMP8.1	Ciliated epithelia-S	RP23-294J17	AAGGGAGAGGAGCTGTTCA	CGATCTGCTCCTCTGTCAGCTGGT
B36	Aldh1L1^{BAC}-Optoα1AR_IRES_lacZ	Glia-E	RP23-7M9	GGGTTGGTCCCGCTATATTC	GAAGGCAGGGATGGTCATAAA

responses, as illustrated in Figure 1. Here, activation of the CatCh2 protein expressed in SA nodal pacemaker cells triggers cardiac conduction, as monitored by GCaMP8 fluorescence in ventricular myocytes. Other combinatorial preparations from the CHROMus toolbox enable the evaluation of cellular function in healthy or diseased animal models. We have constructed 11 mouse lines expressing various optogenetic effector proteins in 7 different lineages and 10 expressing fluorescent GECI reporter proteins in 7 lineages across a wide range of tissues, organs, and systems (Table 1).

Cardiac Conduction System Optogenetic Mice

The potassium/sodium hyperpolarization-activated cyclic nucleotide-gated channel 4 protein (HCN4) underlies the pacemaker current in the sinoatrial (SA) node, controlling heart rate and heart rhythm (DiFrancesco, 1993; Moosmang et al., 2001). For light-activated control of heart rhythm, we constructed a HCN4^{BAC}-CatCh2_IRES_lacZ mouse line, where the expression of the optoeffector CatCh2 and a marker protein (LacZ) are under transcriptional control of the HCN4 locus in a BAC (Table 1), thus directing expression to the cells of the cardiac conductance system. X-gal staining of adult HCN4^{BAC}-CatCh2_IRES_lacZ mice demonstrated specific staining in cells of the cardiac conductance system, including the sinoatrial node region in the right atrium, the atrioventricular junction, and the ventricular conducting network (Figure 2A). LacZ expressing cells were observed at the base of the right carotid vein where it joins the right atrium (Figure 2 – figure supplement 1A) and along the right carotid vein to the base of the common carotid vein (Figure 2 – figure supplement 1B). Expression was also documented in embryonic (E10.5) and neonatal (PN4) hearts in the atrium and the

Figure 1. Combinatorial optogenetic mice. The figure illustrates the general paradigm of tissue specific cellular activation and simultaneous response decoding with tissue specific optical sensors. Here a biallelic SA nodal CatCh2/cardiomyocyte-GCaMP8 mouse is generated from a single cross of isogenic (C57BL/6J), hemi-allelic effector/sensor mice, as in Figure 2H. Mice with specific expression of optoeffectors (cardiac conducting tissue, cardiac and smooth muscle syncytia, endothelium, sympathetic neurons, T cells, and glia) and optosensors (SA nodal tissue, cardiac and smooth muscle, endothelium, ciliated epithelium, and alveolar epithelium) are reported. LA – left atrium, RA – right atrium, RV – right ventricle, LV – left ventricle, Ao – aorta, SVC – superior vena cava, SAN – sinoatrial node. Figure adapted from Virginia Greene.

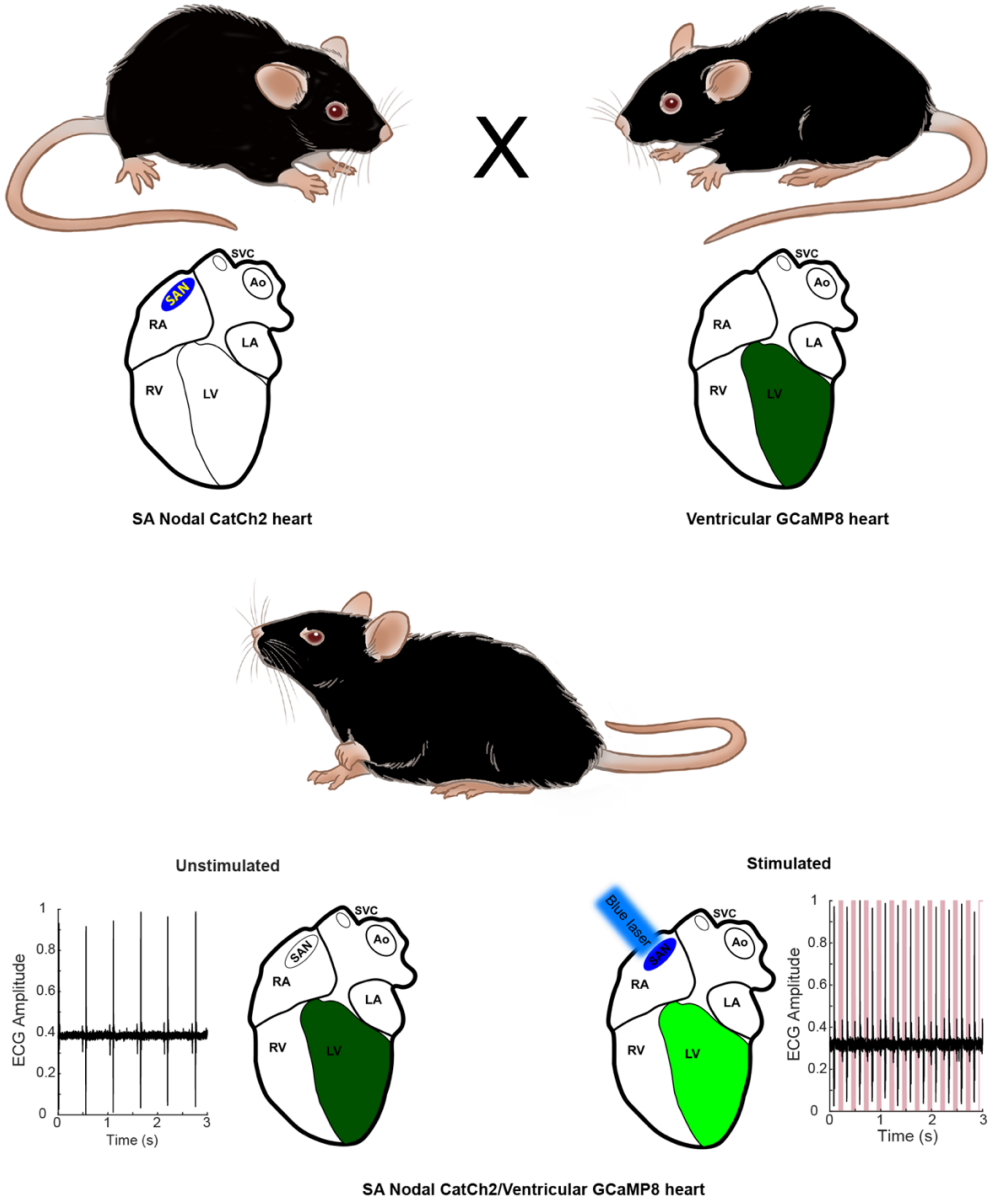

ventricular conducting system (Figure 2B).

To confirm optical control of heart rhythm, we stimulated the SA node area with 473-nm light *in vivo* while recording the ECG. As shown in Figure 2C, cardiac conduction was driven with stimulation between 2Hz and 4Hz, with dropouts at higher frequencies. Heart rhythm returned to normal following optical stimulation (Figure 2 – figure supplement 1C), and illumination of off-target tissue (left ventricle) did not result in optical rhythm control (Figure 2 – figure supplement 1D). Pacing was maintained with laser pulse lengths varying between 15 and 70 ms (data not shown). The increase in laser-stimulated R-wave duration is shown as a widening of the R-wave in the R-wave-centered average of ECG for stimulated and unstimulated beats and the extended PR interval in the P-wave-centered average of ECG sections (Figures 2D, 2F). ECG parameters indicated that R-wave duration and PR interval increased significantly, relative to the autonomously activated cardiac cycle (Figures 2E, 2G), likely indicating a more peripheral activation of SA nodal conducting tissue.

To demonstrate the feasibility of combining optogenetic effector and sensor lines, we crossed HCN4^{BAC}-CatCh2_IRES_lacZ and αMHC-GCaMP8 mice. Pacing by laser stimulation resulted in coupling between optical stimulation and GCaMP8 fluorescence, as shown in Figure 2H, and Supplemental Movie 1. Differences in effector and sensor kinetics must be considered at high stimulation rates, as previously reported (Tallini, Ohkura, et al., 2006). HCN4^{BAC}-CatCh2 mice could also be mated to Acta2^{BAC}-

Figure 2. Cardiac conduction system optoeffector and optosensor mice. **A**, X-gal staining of HCN4^{BAC}- CatCh2_IRES_lacZ adult heart shows LacZ expression in the SA node, AV junction and the ventricular conduction network (arrows). Scale bars – upper panel, 2 mm, lower panels, 300 µm. **B**, Left panel - X-gal staining of wildtype and HCN4^{BAC}- CatCh2_IRES_lacZ E10.5 embryos; upper images – whole embryo, lower images – cardiac region. Right panel - whole heart X-gal staining of neonatal heart showing staining in the cardiac conduction system including the SA nodal region, atrioventricular junction, and ventricle chambers. **C**, ECG recording in an anesthetized HCN4^{BAC}- CatCh2_IRES_lacZ mouse during intravital pacing with laser illumination. ECG recordings from laser activation of CatCh2 protein demonstrate pacing from 2 to 4 Hz (3 Hz not shown), and pacing maximum. **D**, ECG averaged by aligning R-wave peaks during laser-stimulated and unstimulated beats (shading indicates standard deviation, n = 273 stimulated beats, n = 115 unstimulated beats from same mouse as in E), dark and light gray indicate average and standard deviation of laser pulse onset and offset times). Laser power is 32.2 mW, pulse length is 70 ms. **E**, R-wave duration in stimulated and unstimulated beats (****: $p < 0.001$, Mann-Whitney test). Solid lines and dashed lines show median and quartiles. **F**, Averaged ECG aligned by P-wave peak during stimulated and unstimulated beats. **G**, Quantification of PR interval duration shows elongation in stimulated compared to unstimulated beats (****: $p < 0.001$, Mann-Whitney test). **H**, Fluorescent Ca^{2+} measurement during optical stimulation of SA nodal tissue in HCN4^{BAC}-CatCh2_IRES_lacZ /αMHC-GCaMP8 perfused mouse heart at 2 Hz shows combination of optogenetic effectors and sensors through optical pacing of the SA node and fluorescent Ca^{2+} responses from ventricular myocytes. **Top**, fluorescent images from left ventricle with timing of laser pulses indicated by red box. **Bottom**, plot of GCaMP8 intensity from left ventricle in the outlined box (left image). Scale bar – 200 µm. **I**, Expression of GCaMP8 protein in embryonic and adult hearts from HCN4^{BAC}-GCaMP8 mice. Left, anti-GFP immunostaining of paraffin section from E13.5 embryo. Scale bars – 2 mm and 200 µm; right, dorsal view of an adult heart showing native GCaMP8 fluorescence in the SA nodal region, the right carotid vein and the base of common carotid vein. RA - right atrium, CCV - common carotid vein, RCV - right carotid vein, LV - left ventricle, and RV - right ventricle.

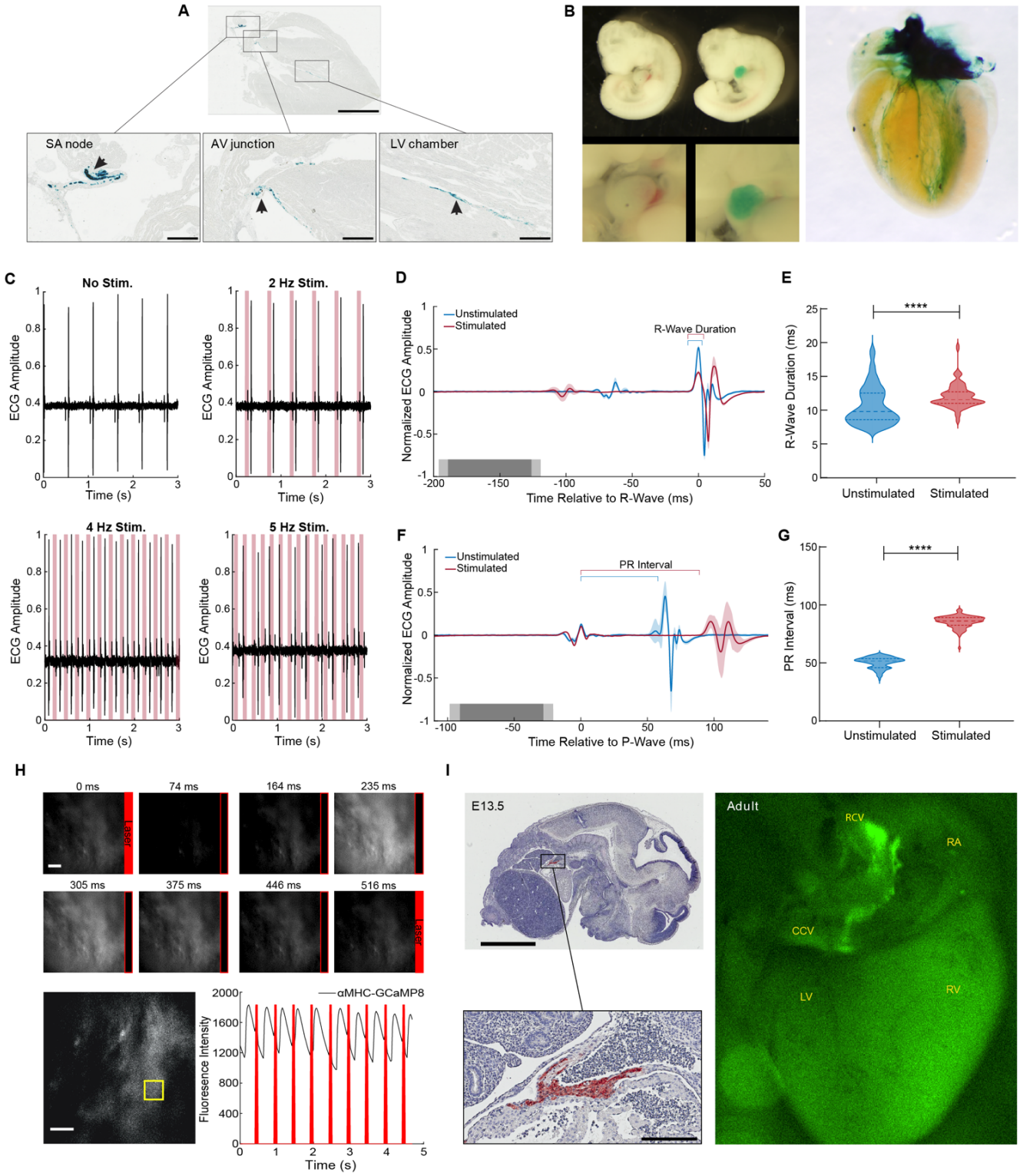
A
SA node
AV junction
LV chamber
B
C
No Stim.
2 Hz Stim.
4 Hz Stim.
5 Hz Stim.
ECG Amplitude
Time (s)
D
Unstimulated
Stimulated
R-Wave Duration
Normalized ECG Amplitude
Time Relative to R-Wave (ms)
E
****
R-Wave Duration (ms)
Unstimulated
Stimulated
F
PR Interval
Time Relative to P-Wave (ms)
G
PR Interval (ms)
H
0 ms
74 ms
164 ms
235 ms
305 ms
375 ms
446 ms
516 ms
Laser
αMHC-GCaMP8
Fluoresence Intensity
I
E13.5
Adult
RCV
RA
CCV
LV
RV

GCaMP5_mCherry (Figure 4) and Cdh5^{BAC}-GCaMP8 lines (Figure 6) to study smooth muscle or endothelial cell responses to the cardiac pacing.

For the study of the development of the cardiac conduction system and disturbances of conduction in disease states, we developed a HCN4^{BAC}-GCaMP8 mouse line. GCaMP8 is expressed in the *sinus venosus* (Figure 2I, left panels) of the embryonic heart and in the SA nodal area at the junction of right atrium and right carotid vein in the adult heart, extending down to the base of the common carotid artery (Figure 2I, right panel), similar to the expression pattern in HCN4^{BAC}- CatCh2 mice (Figure 2 – figure supplement 1B). In developing embryos, spontaneous GCaMP8 signaling was observed in the heart at embryonic day (E) 8.5, E10.5, and E13.5, as well as at postnatal day (PN) 4 (Figure 2 – figure supplement 2A). Conduction of the GCaMP8 fluorescence signal was observed moving from the atrium to the ventricle in the E13.5 embryo (Supplemental Movie 2). In the adult heart, GCaMP8 signaling was observed prior to spontaneous ventricular contractions (Figure 2 – figure supplement 2B, Supplemental Movie 3).

<u>Cardiac Myocyte Optogenetic Mice</u>

We constructed two optogenetic lines designed to study Ca^{2+} signaling and electrical communication between heart cells using a minimal promoter for αMHC protein (Gulick, Subramaniam, Neumann, & Robbins, 1991). In order to optically initiate cardiac dysrhythmias at virtually any surface region of the heart, we developed the αMHC-CatCh2_IRES_lacZ strain, which expresses the CatCh2 and LacZ transgenes in

cardiomyocytes. X-gal stained cryosections of the heart showed widespread staining of throughout the heart (Figure 3A). Laser irradiation (473 nm) of the left ventricle enabled the stimulation of ventricular premature activations at lower frequencies, and complete ventricular pacing at 8 Hz; above 8 Hz pacing was lost but irregular ventricular initiation could be produced, consistent with the refractory period of ventricular myocytes (Figure 3B). As predicted for ventricular activation, the ECG showed markedly enhanced QRS duration without corresponding P-waves, as visualized in an R-wave-centered average of ECG sections for stimulated and unstimulated beats in three mice (Figure 3C). Differences in ECG morphology among animals at baseline, as well as unsuccessful stimulation for some beats accounts for high variability and abnormal morphology in the averaged trace. The mean R-wave duration significantly increased upon laser stimulation compared to the native unstimulated heartbeat in all three mice examined (Figure 3D). Higher magnification ECG traces of autonomous heart activation following ventricular laser stimulation show typical widened QRS complexes (red) followed by return to normal heart activation (Figure 3E, 3F).

We also created the αMHC-GCaMP8 line to enable visualization of *in vivo,* real-time, cardiac Ca^{2+} responses under different experimental stimuli and disease conditions. Cryosections from the heart revealed widespread GCaMP8 fluorescence and immunoreactivity in hearts from this line (Figure 3G). To obtain high resolution intravital images of a beating heart, we injected Texas Red-conjugated dextran retro-orbitally to label the vasculature and acquired two-channel, two-photon images of the left ventricle (Figure 3H). GCaMP8 Ca^{2+} fluorescence was observed in cardiomyocytes in the

Figure 3. Cardiomyocyte optoeffector and optosensor mice. A, X-gal staining of cardiomyocytes in αMHC-CatCh2_IRES_lacZ, scale bar – 200 and 60 μm. **B**, ECG recording during intravital laser stimulation of the CatCh2 protein in the left ventricle at various frequencies (laser power is 32.2 mW, average pulse length is 14 ms). **C**, R-wave centered average of all stimulated and unstimulated beats shows R-wave widening (shading indicates standard deviation of ECG signal, dark and light gray indicate average and standard deviation of laser pulse onset and offset times). **D**, R-wave durations with and without laser stimulation of the transgenic CatCh2 protein are shown from three different mice. **E**, ECG recordings demonstrating transition from autonomous to laser-stimulated conduction. **F**, Premature ventricular contractions evoked by laser stimulation of αMHC-CatCh2 ventricular myocytes. **G,** Expression of GCaMP8 in heart of an adult αMHC-GCaMP8 mouse; **top**, native fluorescence, **bottom**, anti-GFP immunohistochemistry, scale bars - 200 μm. **H**, Intravital two-photon microscopy of the αMHC-GCaMP8 heart. Frames from a three-dimensional reconstruction of αMHC^{BAC}-GCaMP8 fluorescence over a cardiac cycle. Each frame represents a 10% increment of the cardiac cycle defined by the peak of the R-wave. The x-axis is the anterior to posterior direction, the y-axis is the apex to base direction, and the z-axis is the epicardium to endocardium direction of the left ventricle free wall; 166 x 166 x 100 μm (xyz) region shown. GCaMP8 fluorescence in cardiomyocytes (green); vasculature labeled with Texas Red conjugated dextran (magenta). **I**, Average and standard deviation of change in fluorescence intensity of the imaged region demonstrating Ca^{2+} transients during the cardiac cycle.

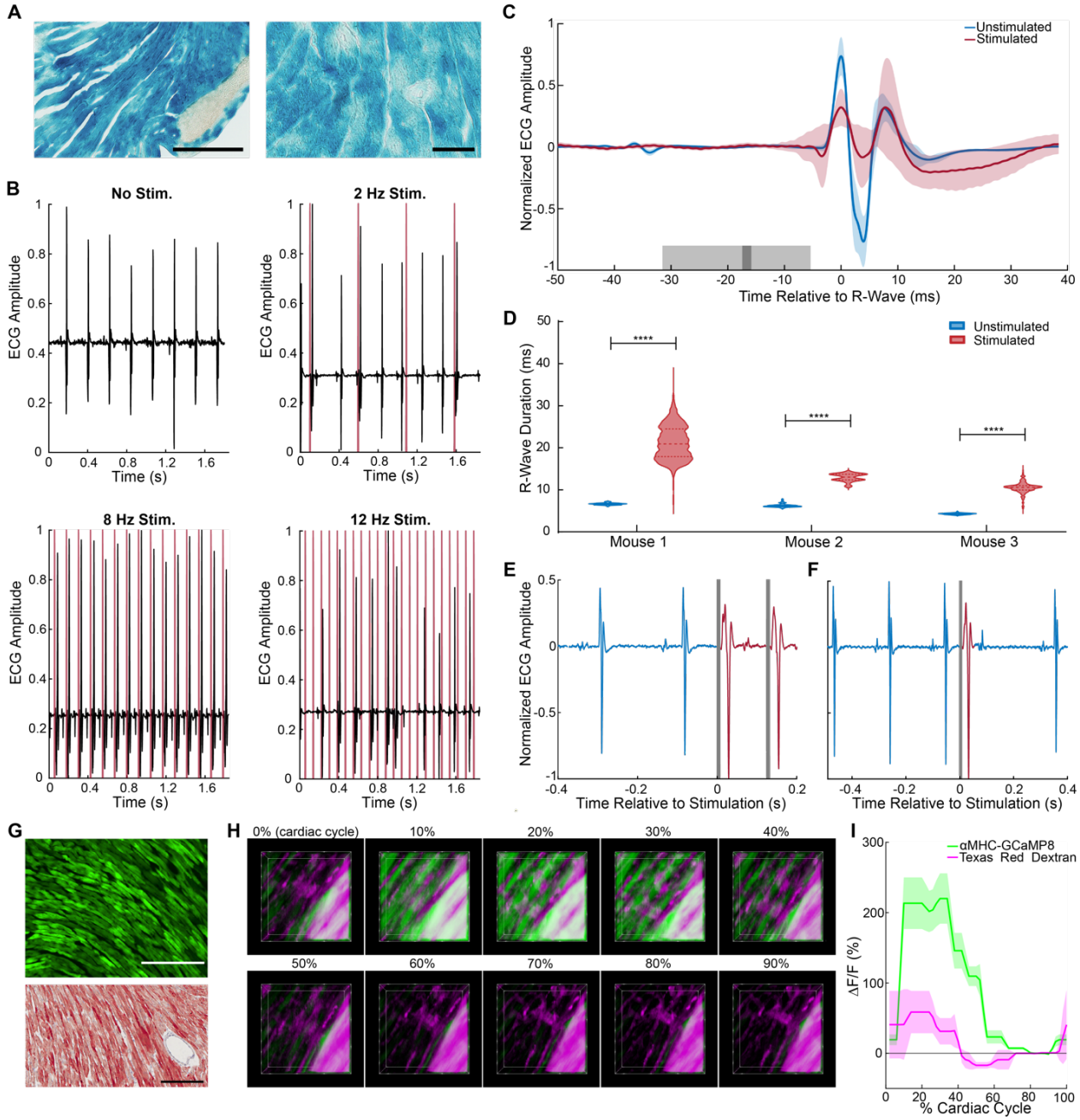
A
B
No Stim.
2 Hz Stim.
8 Hz Stim.
12 Hz Stim.
ECG Amplitude
Time (s)
C
Unstimulated
Stimulated
Normalized ECG Amplitude
Time Relative to R-Wave (ms)
D
R-Wave Duration (ms)
****
Mouse 1
Mouse 2
Mouse 3
E
F
Time Relative to Stimulation (s)
G
H
0% (cardiac cycle)
10%
20%
30%
40%
50%
60%
70%
80%
90%
I
αMHC-GCaMP8
Texas Red Dextran
ΔF/F (%)
% Cardiac Cycle

stabilized ventricular free wall during the normal cardiac cycle, coincident with heart contractions. The vascular dextran fluorescence signal reports only motion-related fluorescence changes (Figure 3I, Supplemental Movie 4).

Smooth Muscle Optogenetic Mice

We constructed optogenetic effector and sensor BAC transgenic mice using transcriptional activity from a region that spanned the smooth muscle specific α-Actin2 gene, which is selectively expressed in smooth muscle (Mack & Owens, 1999). Sensor lines expressing GCaMP (5 or 8.1) and RCaMP1.07 fluorescent Ca^{+2} reporters, and effector lines expressing the optoα1AR (Airan et al., 2009), optoß2AR (Airan et al., 2009), and CatCh2 (Zhang et al., 2006) proteins, were developed under smooth muscle specific transcriptional control.

We engineered three recombinant BAC constructs to drive expression of red or green-red sensors in smooth muscle cells (Table 1 – figure supplement 1). The $Acta2^{BAC}$-RCaMP1.07 (Bethge et al., 2017) line expresses the sensor selectively in arterial smooth muscle (Figure 4 – figure supplement 1A, upper panels). *In vivo* imaging revealed cyclic fluorescence increases associated with contractions of the right atrium (Figure 4 – figure supplement 1A, lower panel; Supplemental Movie 5). When used with optoeffector mice, the line eliminates spectral overlap with excitation of GFP -based sensors.

Acta2^{BAC}-GCaMP5_mCherry mice provide the advantage of ratiometric Ca^{2+} determination, as well as ease of expression determination *in vivo.* As shown in brain surface vessel images (Figure 4A upper panel), the GCaMP5_mCherry fusion protein is strongly expressed in the arterial system extending to the arteriolar-capillary junctional cells, but not in the capillary network. To further enhance the intensity of red fluorescence, we created a second dual color sensor line using the same transcriptional strategy, but substituting mVermilion, a novel monomeric mCherry variant with a two-fold increase in brightness but equivalent excitation and emission profiles. The Acta2^{BAC}-GCaMP8.1_mVermilion displayed a similar expression pattern (Figure 4A – lower panel). *In vivo* experiments with these lines indicated robust smooth muscle Ca^{2+} dependent fluorescence. Contractions of blood vessels, airways, and gastrointestinal organs demonstrated increases in green fluorescence during muscle contraction. As shown in Figure 4 – figure supplement 1B and Supplemental Movie 6, *in vivo* fluorescent imaging of spontaneous contractions in the large intestine showed a wave of GCaMP5 signaling in the longitudinal muscles that was coupled to contractions, whereas mCherry fluorescence remained constant (data not shown).

We constructed three effector lines for smooth muscle optical activation using the Acta2 BAC (RP23-370F21; Table 1) and examined the expression of the LacZ protein located downstream of the optogenetic effector coding sequence in different tissues from Acta2^{BAC}-Optoα1AR_IRES_lacZ, Acta2^{BAC}-Optoß2AR_IRES_lacZ and Acta2^{BAC}-CatCh2_IRES_lacZ mice by X-gal staining. The staining data shows widespread expression of all 3 constructs in the brain arterial system (Figure 4B), including the

Figure 4. Smooth muscle optoeffector and optosensor expression. **A,** Native fluorescence of surface blood vessels from Acta2^{BAC}-GCaMP5_mCherry (upper) and Acta2^{BAC}- GCaMP8.1_mVermilion brain (lower). Note the absence of fluorescence in veins (arrows). Left panel -overlay, right panels – red and green channels. **B,** X-gal staining of brain surface arteries from Acta2 optoeffector mice. All images shown are representative images from 3 animals unless otherwise specified.

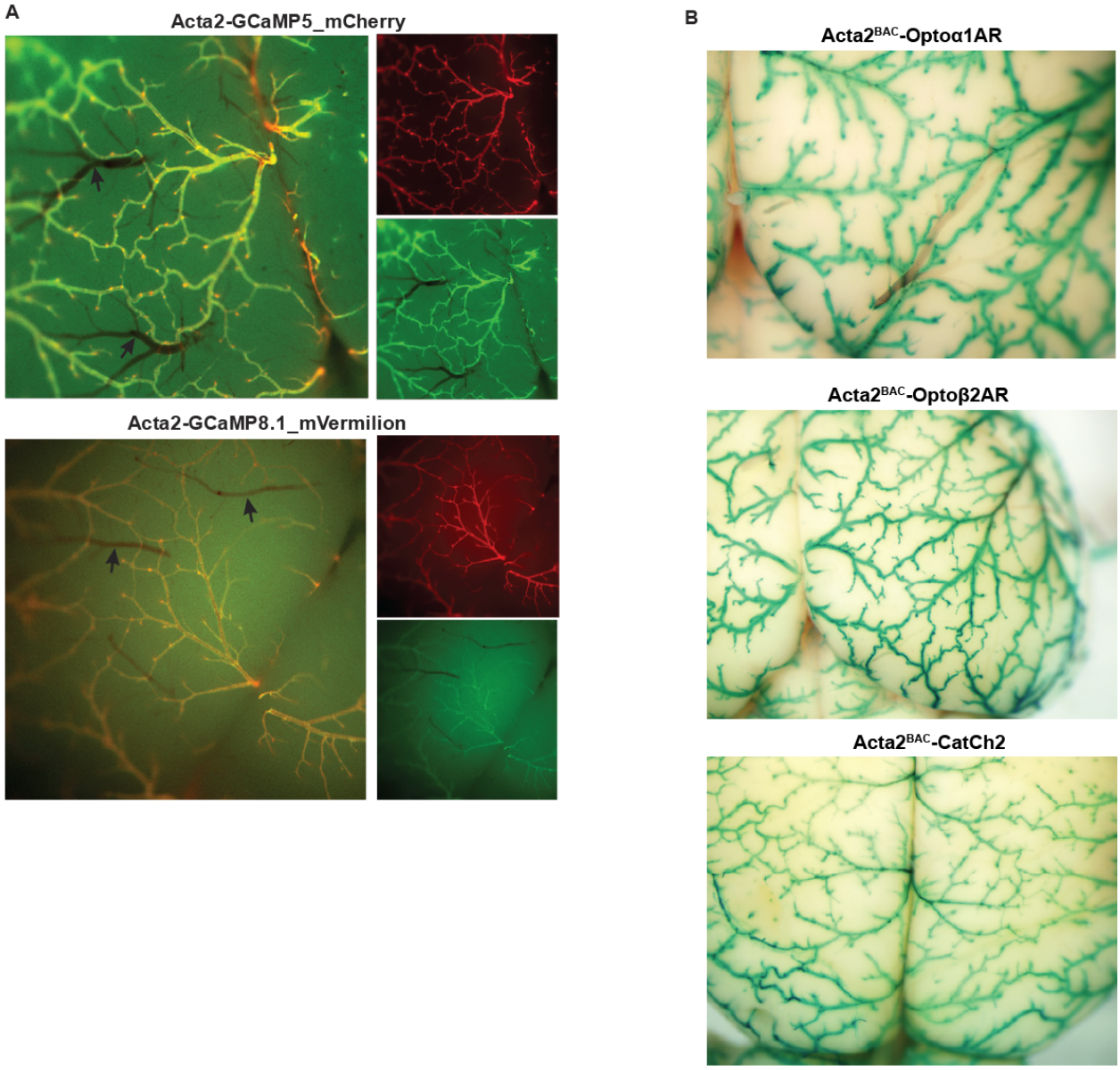

arteriolar/capillary junction. LacZ activity was also observed in arteries supplying the diaphragm, smooth muscles surrounding coronary blood vessels, the bladder, bronchiolar and vascular smooth muscles in lung, and other tissues such as the small intestines, kidney and uterus (data not shown). X-gal staining of a non-transgenic littermate did not detect LacZ activity (Figure 4 – figure supplement 1C).

As receptor -mediated activation of phospholipase C or adenylyl cyclase (with associated increases in $InsP_3$ or cAMP) mediates smooth muscle contraction and relaxation respectively, we examined constriction or dilation of isolated cerebral and mesenteric arteries in response to optical activation of the chimeric Optoα1AR and Optoß2AR proteins. Brief exposure of arteries isolated from Acta2^{BAC}-Optoα1AR_IRES_lacZ mice to 405nm light resulted in vasoconstriction (Figure 5A, left panel), while light -activated arteries from Acta2^{BAC}-Optoß2AR_IRES_lacZ lines underwent slow dilations (Figure 5A, middle panel; Supplemental Movie 7), demonstrating functional expression of the proteins and expected physiologic responses. The activation of channelrhodopsin in arteries isolated from Acta2^{BAC}-CatCh2_IRES_lacZ mouse resulted in rapid constriction (Figure 5A, right panel; Supplemental Movie 8).

Optoeffector coupling was demonstrated at a cellular level in whole-cell, voltage clamped arterial myocytes. We first examined coupling through the known linkage between cAMP/Protein Kinase A signaling and voltage-gated potassium channels in arterial myocytes (Johnson et al., 2009; Luykenaar & Welsh, 2007; Nelson & Quayle,

1995; Wellman, Santana, Bonev, & Nelson, 2001). Macroscopic I_K currents from single voltage-clamped myocytes isolated from male mesenteric and mid-cerebral arteries were recorded before and after photo-activation of Optoß2AR. I_K (composed of Kv1, Kv2.1, and BK currents) was activated at 10 s intervals by the application of a 500 ms step depolarization from the holding potential of -70 mV to +60 mV. Activation of the Optoß2AR protein by 488 nm light increased the amplitude of I_K 10 s after the exposure, reaching a higher, relatively stable plateau approximately 80 s after photoactivation (Figure 5B). Although the dispersion of I_K amplitudes increased about 150 s after activation of Optoß2AR, I_K remained higher than under control conditions for at least 500 s. Exposure to a second and third pulse of light had limited additional effects, suggesting that the initial Optoß2AR-induced potentiation of I_K was near maximal. In five similar experiments in mesenteric myocytes, Optoß2AR photoactivation increased I_K 1.15 ± 0.04-fold at +60 mV, and 1.23 ± 0.05-fold in cerebral arterial myocytes.

Similarly, CatCh2 optical activation was examined in cerebral and mesenteric arteries by recording membrane currents at -70 mV before and after illumination (488 nm, 50ms pulses at 1 Hz). As shown in Figure 5C, optical stimulation repeatedly evoked fast inward currents that terminated as soon as the laser was turned off. In the representative cerebral myocyte shown, the amplitude of the evoked current was about 75 pA, and subsequent light pulses evoked stable I_{Cat} with an amplitude of 68 ± 1 pA, suggesting that under our experimental conditions there is a relatively small level of inactivation of CatCh2 channels (Figure 5C, upper panel). Longer light pulses produced a larger inward current (~125 pA) that quickly (~100 ms) decayed to a lower amplitude

Figure 5. Smooth muscle optoeffector function. **A,** Activation of optogenetic proteins in effector lines results in either vessel contraction (Acta2^{BAC}-Optoα1AR-_IRES_lacZ – left panel, Acta2^{BAC}-CatCh2_IRES_lacZ –right panel) or relaxation (Acta2^{BAC}-Optoß2AR_IRES_lacZ – middle panel). **B,** Laser activation of transgenic Optoß2AR proteins induces K currents in isolated arterial myocytes. Upper panel – mesenteric myocytes, lower panel –cerebral myocytes. **C,** Laser activation of transgenic CatCh2 protein induces inward membrane current. Upper panel – repeated laser pulses result in rapid inward current in cerebral myocytes. Middle panels – long pulses achieve a steady state inward current in cerebral (upper) and mesenteric myocytes (lower) after an initial spike only on the first pulse. Bottom panel – activation of cerebral myocytes results in higher initial and steady state current compared to mesenteric myocytes. Optoß2AR data were derived from 5 cells isolated from 3 mice and the CatCh2 data were generated from 8 cells isolated from 5 mice.

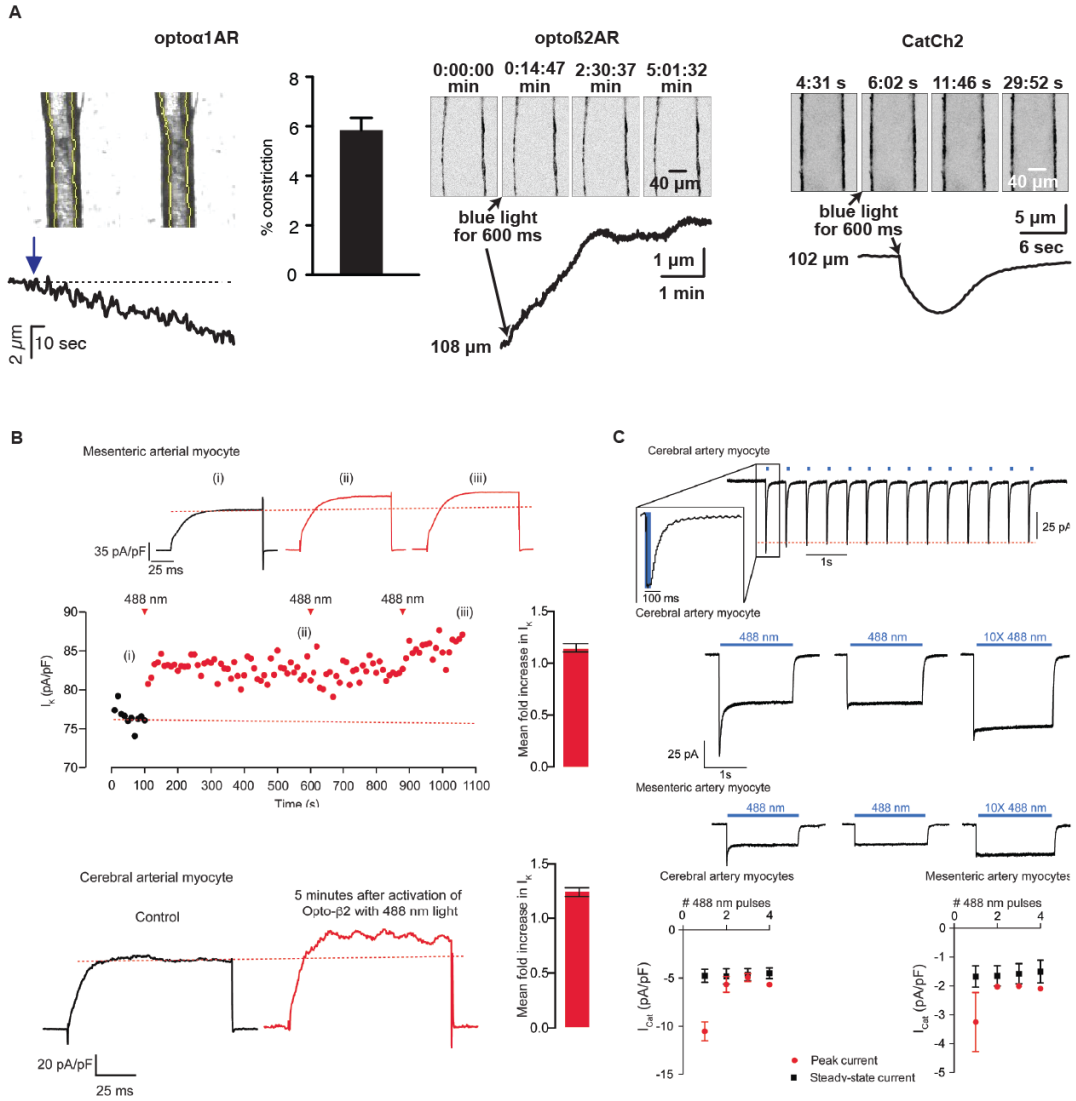

(~35 pA) plateau, remaining relatively constant as long as the laser was turned on. This I_{Cat} quickly terminated (<100 ms) after the laser was turned off. Notably, a second 488 nm light pulse to the same cell evoked an I_{Cat} that lacked the high-amplitude transient component of the first light pulse but had the amplitude and kinetics of the steady-state I_{Cat} in the first pulse. Similar observations were made in isolated mesenteric myocytes (Figure 5B, middle panels). The activation of cerebral myocytes resulted in higher currents compared to mesenteric arteries and repeated pulses resulted in dampened initial inward current (Figure 5B, bottom panels). Thus, Acta2 optoeffector lines express functional chimeric receptors and channel proteins, enabling optical modulation of smooth muscle signaling in a variety of experimental conditions.

Endothelial Optogenetic Mice

To enable studies of the interactions between endothelium and surrounding perivascular cells we created three BAC transgenic optogenetic effector, and one fluorescent reporter, mouse lines using the endothelial cell specific cadherin5 gene locus. As with smooth muscle, Optoα1AR, Optoß2AR, and CatCh2 cDNAs and LacZ ORF were targeted to the Cdh5 initiation codon, with an IRES and the LacZ sequence downstream of the optoeffectors. X-gal staining revealed wide expression in endothelial cells of the heart (Figure 6A), brain (Figure 6 – figure supplement 1A), and other tissues (Figure 6 – figure supplement 1B). Similarly, GCaMP8 selective expression in endothelial cells was achieved in Cdh5^{BAC}-GCaMP8 mice (Figure 6B, Figure 6 – figure supplement 1C). Endothelial GCaMP8 signal was sufficiently bright to be observed in coronary microvasculature using intravital 2-photon microscopy (Figure 6C).

Figure 6. Endothelial cell optoeffector and optosensor expression. **A,** X-gal staining of heart cryosections from Cdh5^{BAC}-Optoα1AR_IRES_lacZ, Cdh5^{BAC}-Optoß2AR_IRES_lacZ and Cdh5^{BAC}-CatCh2_IRES_lacZ mice. Scale bars - 200 microns. **B,** Native fluorescence of GCaMP8 protein in heart cryosection (left panel) and brain dorsal surface (right panel). Scale bar - 200 µm. **C,** Intravital 2-photon imaging of Cdh5 ^{BAC}-GCaMP8 mice shows endothelial GCaMP8 (green) labelling of coronary microvasculature. Intravenous Texas-Red conjugated 70-kDa dextran identifies the vessel lumen (magenta). All images shown are representative images from 3 animals unless otherwise specified.

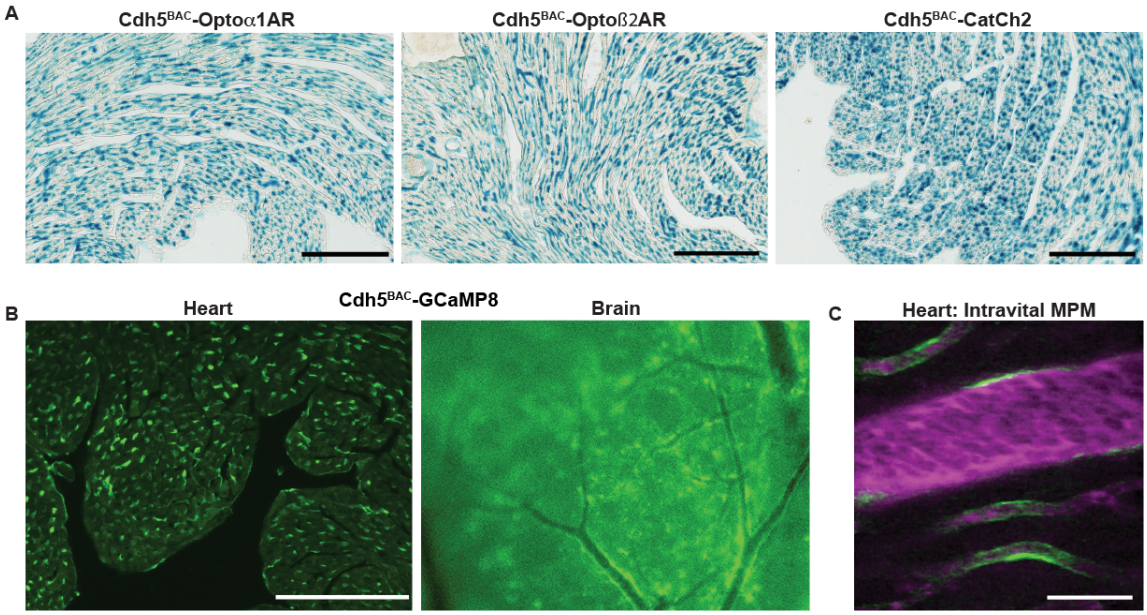

To confirm functional expression of optoeffector proteins, we deployed several analyses. First, we examined endothelium -induced vasodilation that occurs secondary to the release of Ca^{2+} and synthesis of NO in EC (Straub, Zeigler, & Isakson, 2014). Optical activation of femoral arteries in Cdh5^{BAC}-Optoα1AR_IRES_lacZ mice *in vivo* resulted in marked vasodilation, whereas laser stimulation alone caused a slight vasoconstriction in control arteries (Figure 7A). Similar results were obtained in cremaster arteries, but not in control arteries (Figure 6 – figure supplement 1D). We also examined the propagation of arterial dilation that occurs following muscarinic stimulation (Tallini et al., 2007), and is difficult to separate from agonist diffusion (Welsh & Segal, 1998). Laser stimulation triggered bidirectional arterial dilation at points distal to the laser beam, with a delay in the onset of vasodilation and attenuation of the amplitude (Figure 7B). Vasodilation was triggered at 32.2mW, but not at lower laser powers (Figure 7C). Photoactivation of chimeric ß2 adrenergic receptors in Optoß2AR mice also triggered vasodilation (Figure 7D). Interestingly, ß2AR -mediated dilation did not result in conducted dilation distal to the point of laser stimulation as observed in Optoα1AR mice.

<u>Other Optogenetic Lines</u>

The gap junction protein connexin40 (Cx40) is expressed in specialized cells of the cardiac conduction system and in arterial endothelial cells, and expression in embryonic myocytes is critical for heart function prior to development of a mature conduction system (Delorme et al., 1995). To facilitate improved studies of embryonic and adult cardiac conduction defects, as well as physiologic vasomotor control, we created a

Figure 7. Endothelial cell optoeffector function. **A,** Laser stimulation of femoral artery in Cdh5^{BAC}-Optoα1AR induces vasodilation. Left panel – MATLAB generated 3D rendering of vessel width and intensity over time. The arrowheads mark the start and end of laser activation and the asterisk marks dilation of the artery. Right panel – Comparison of peak change in vessel width between Cdh5^{BAC}-Optoα1AR_IRES_lacZ and C57BL/6J control mice, n = 3 both groups. **B,** Activation of Optoα1AR protein results in migration of vasodilation away from the laser irradiation point. Left panel – bright field image of the femoral artery with positions of the mid, right (Rt) and left (Lf) analysis positions indicated. Red dashed circle indicates laser irradiation spot on the vessel. Right panel – change in vessel width over time. **C,** Vessel relaxation is dependent on laser intensity. **D,** Comparison of vasodilation induced by Optoα1AR and Optoß2AR proteins with laser power at 32.2 mW.

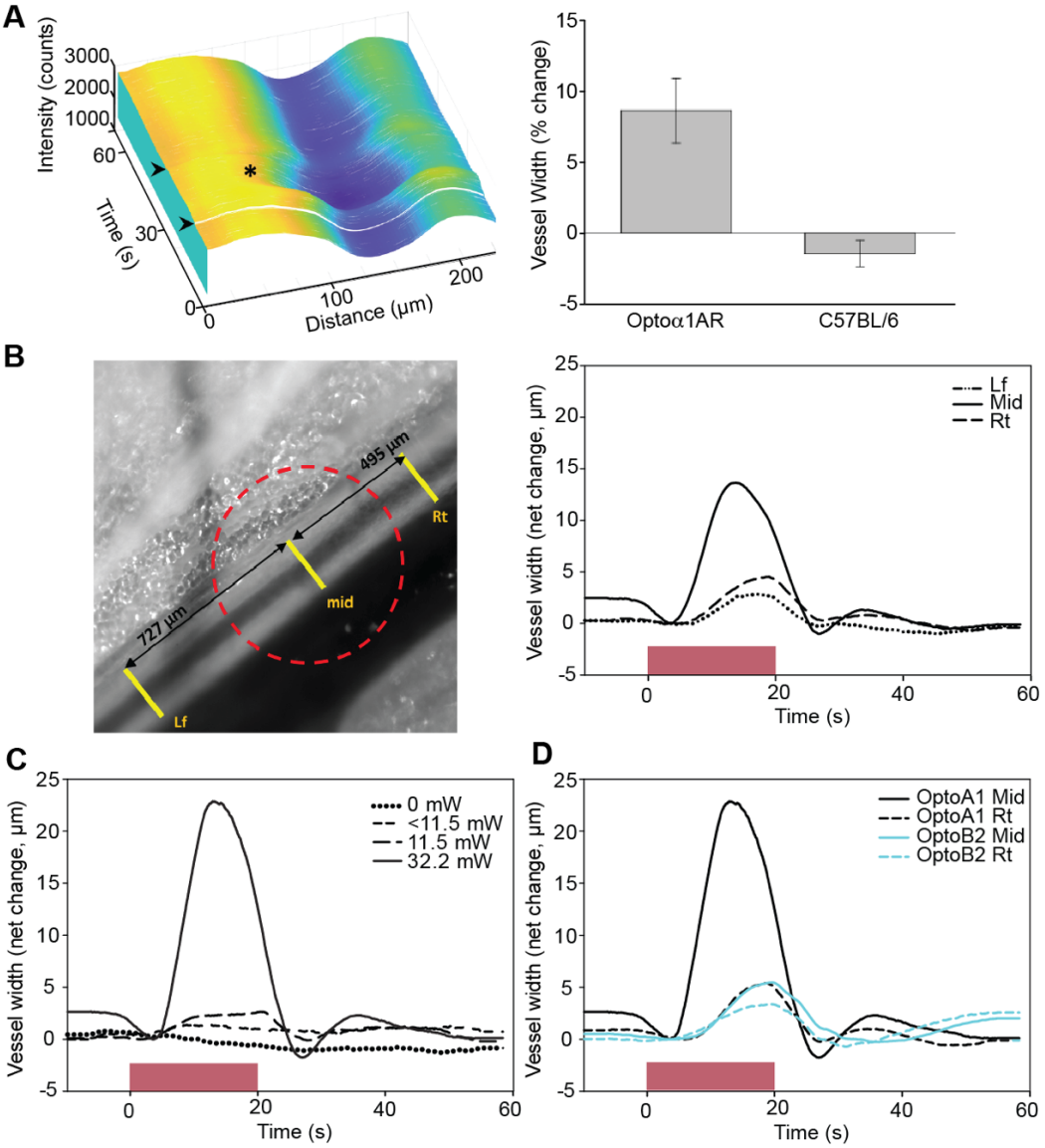

Cx40^{BAC}-GCaMP5_mCherry mouse line. The ratiometric green-red fusion protein is expressed in arterial endothelia from the kidney, the ventricular conductance system and atrial myocytes (Figure 8A), and in arterial endothelial cells (Figure 8 – figure supplement 1A). To extend studies to the sympathetic nervous system, we used the dopamine ß-hydroxylase locus to target optogenetic effectors to peripheral neurons and adrenal medulla cells (reviewed in Gonzalez-Lopez and Vrana, 2019 (Gonzalez-Lopez & Vrana, 2020)). X-gal staining of adult brain and adrenal glands of Dbh^{BAC}-CatCh2_IRES_lacZ demonstrated the expression of LacZ in the *locus coeruleus* (Figure 8B) and adrenal medulla (Figure 8 – figure supplement 1B). BAC DNA from the aldehyde dehydrogenase family 1 L1 (Aldh1L1) gene locus was similarly used to target glial cells. Aldh1L1^{BAC}-Optoα1AR_IRES_lacZ mouse express in cerebellar (Figure 8C) and olfactory regions in the brain and the kidney (Figure 8 – figure supplement 1C). The expression of Optoα1AR protein in immune cells was targeted using a BAC containing the Lck gene to facilitate studies on $InsP_3$ activation in T-lymphocytes. X-gal staining for LacZ expression indicates optoeffector expression in the spleen (Figure 8D). Mice expressing GCaMP8.1 protein in FoxJ1$^+$ cells were developed using BAC RP23-294J17 (Table 1). Immunostaining analysis with anti-GFP antibody indicated GCaMP8.1 expression in the bronchioles, trachea, and the testis (Figure 8E). We constructed the SP-C^{BAC}-GCaMP8 mouse to target reporter expression in Type II alveolar cells. Anti-GFP antibody analysis of lung sections indicated wide distribution of GCaMP8 expression (Figure 8 – figure supplement 1D).

Figure 8. Characterization of other CHROMus mouse lines. A, Anti-GFP IHC of Cx40^{BAC}-GCaMP5_mCherry mouse. GCaMP5 is expressed in the atrioventricular junction (AVJ) region, atrial myocytes (AM) (left panel) and cells lining the endocardium in the adult heart (middle panel; scale bars – 200 µm) and the renal artery (right panel; scale bar – 60 µm). **B,** X-gal staining of adult brain sagittal section from Dbh^{BAC}-CatCh2_IRES_lacZ mouse showing LacZ expression in the *locus coeruleus* region. Box outlines area of enlargement. CB – cerebellum, LC – *locus coeruleus*. Scale bars; top panel – 500 µm, bottom panel – 200 µm. **C,** X-gal staining of cerebellar region from Aldh1L1^{BAC}-Optoα1AR_IRES_lacZ mouse. Box outlines area of enlargement. Scale bars; top panel -2 mm, bottom panel – 200 µm. **D**, X-gal staining of spleen from Lck^{BAC}-Optoα1AR_IRES_lacZ mouse. Inset image shows X-gal staining from a wildtype littermate control. Scale bars – 300 µm, inset – 600 µm. **E,** Anti-GFP IHC of lung, trachea and testis tissues from FoxJ1^{BAC}-GCaMP8.1 mouse. Scale bars – 200 µm. All images shown are representative images from 3 animals unless otherwise specified.

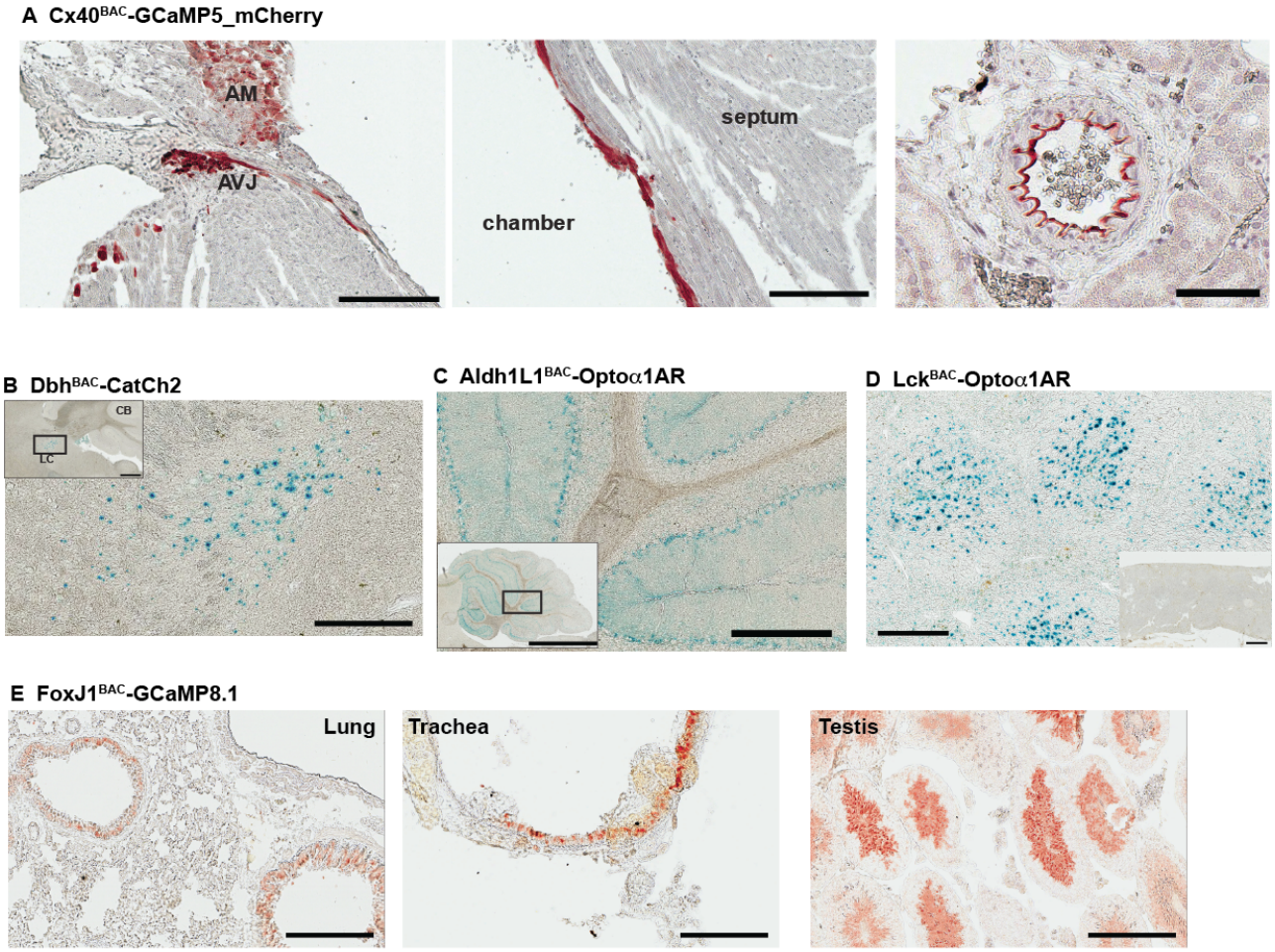

Discussion

We have generated 21 lines of optogenetic sensor and effector mice, in which the expression of the optogene is lineage specified in cardiovascular and related cell lineages (Table 1), and sensor/effector pairs can be combined through simple, monoallelic crosses. More broadly, the lines facilitate the combination of two technologies, each with enormous potential for use in the dissection of signaling processes in complex multicellular systems: genetically encoded optical sensors (Kotlikoff, 2007; Nakai & Ohkura, 2003; Tsien, 2003) and effectors (Fenno et al., 2011). Individually, these technologies have advanced our understanding of physiological *in vivo* processes; combined, biallelic effector/reporter mice constitute a novel platform for the activation and detection of cellular signaling *in vivo*. These new mouse lines comprise a publicly available molecular toolbox that enables investigators to generate physiologically relevant mono- or multiallelic transgenic mice tailored to their research interests, without the need for requisite technical expertise and financial commitment associated with constructing transgenic mice. The monoallelic nature of these lines also facilitates crosses with mouse models of cardiovascular disease. All mice are available as part of a collaborative effort between Cornell/National Heart Lung Blood Resource for Optogenetic Mouse Signaling (CHROMus) and The Jackson Laboratory.

Previous approaches have developed, or exploited, available *Cre* recombinase driver mice to confer tissue specific expression of fluorescent markers or optogenetic sensors downstream of LoxP-STOP-LoxP sequences (Madisen et al., 2010; Zariwala et al., 2012). While this approach has the advantage of using previously characterized Cre

lines and can use strong promoter sequences to drive optogenetic protein expression, there are several important drawbacks to this approach. These include variable penetration of the Cre-mediated recombination at LoxP sites within the target cells, limited specificity of non-BAC Cre promoters (Madisen et al., 2010), and the inefficient process of producing bi-allelic mice for experiments. The latter drawback excludes, for practical purposes, one of the most important advantages of the use of optogenetic mice – crosses with genetic strains or mutant lines that mimic human disease. The use of Cre/Lox approaches for such experiments requires complicated and inefficient breeding strategies. The strains reported here provide direct, tissue -specific expression of optogenetic proteins and enable simple mating strategies for the development of biallelic mice.

Separate targeting of cardiac conducting cells and myocytes enabled light-activated heart activation, and we demonstrate activation of the heart either through stimulation of cells within the SA node (Figure 2), or extra-conduction system activation equivalent to premature ventricular contractions (Figure 3). By crossing nodal optoeffector ($HCN4^{BAC}$-CatCh2_IRES_lacZ) and myocyte sensor (αMHC-GCaMP8 strains) mice, we demonstrate the feasibility of combinatorial optogenetics and report the ability to activate and detect heart signaling (Figure 2H, and the Supplemental Movie 1). We also demonstrate the ability to selectively examine cardiac conduction using $HCN4^{BAC}$-GCaMP8 mice, and their robust signaling of conduction events in embryonic, neonatal, and adult hearts (Figure 2). The cardiac GCaMP8 sensor lines represent several improvements, as they exploit recent structure-based improvements in circular

permutation of GFP (Ohkura et al., 2012; Tian et al., 2009), resulting in higher brightness and dynamic range. Conduction failures result in the implantation of more than 200,000 pacemakers annually in the United States alone (Mond & Proclemer, 2011), and the ability to selectively initiate cardiac conduction at local sites within the heart (optoeffector lines), either through activation of specialized conducting cells or myocytes, and to monitor activation of the conduction system (optosensor lines), confers significant experimental advantages both in understanding conduction system failure and strategies to develop biological pacemakers (Meyers, Jay, & Rentschler, 2016; Nyns et al., 2019; Vedantham, 2015). Similar approaches can be envisioned for studies of heart failure, a major cause of mortality world-wide (Bui, Horwich, & Fonarow, 2011). Two areas of specific value would be the understanding of cardiomyopathy induced arrhythmias (Asimaki, Kleber, MacRae, & Saffitz, 2014) and cell and gene-based approaches to therapy (Nakamura & Murry, 2019).

The development of mouse lines with robust expression of optical effectors and sensors in smooth muscle and endothelial cells provides similar experimental advantages for vascular biology. We report the first mice conferring lineage specific expression of sensors that allow light activated depolarization through CatCh2 channels or release of intracellular Ca^{2+} through Optoα1AR, chimeric α- adrenoceptors, as well as relaxation of smooth muscle through photoactivation of Optoß2AR, chimeric ß2 receptors. Interestingly, we observed rhythmic endothelial cell signaling during the cardiac cycle, enabling dissection of mechanisms that regulate blood flow, matching perfusion to metabolic demand (Duncker & Bache, 2008). Similar approaches have led to important

advances in the understanding of metabolic vascular coupling in the brain and other arterioles (Gonzales et al., 2020; Sonkusare et al., 2012; Sonkusare et al., 2014), but studies in the heart face additional imaging challenges associated with imaging the beating heart. We used stabilized optical windows and deconvolution approaches to address these challenges (Figs. 2 and 3). The creation of lines that enable ratiometric measurements (Acta2^{BAC}-GCaMP5_mCherry and Acta2^{BAC}-GCaMP8.1_Vermilion; Fig. 4) add additional experimental advantages in this regard. Similarly, the ability to initiate synthesis of critical smooth muscle second messengers through the expression of light sensitive chimeric receptor proteins fused to catalytic domains of α1 and ß2 adrenoceptors (Airan et al., 2009) provides important capabilities to probe vascular control mechanisms in smooth muscle tissues, and the ability to control the synthesis in an individual cell type.

Finally, we report additional lines that enable studies of sympathetic neurons, glial cells, and Type II alveolar cells. These lines show robust, tissue -specific expression of the optoeffector or optosensor proteins, enabling similar studies of neurovascular and lung cell signaling.

In summary, BAC transgenic optogenetic effector and sensor lines provide novel experimental platforms for real-time *in vivo* investigations of molecular signaling in complex physiological systems. The mice are available to experimenters through JAX and represent a tool kit that can advance the use of optogenetics in a wide array of experimental investigations.

Materials and Methods

Animal Protocols.

All animal protocols were reviewed and approved by the Cornell University Institutional Animal Care and Use Committee (IACUC) and by University of California, Davis IACUC in accordance with the National Institutes of Health Guide for the Care and Use of Laboratory Animals.

Availability of mouse lines

Please see the Major Resources Table in the Appendix.

Construction of transgenic mice

Mouse lines were created by injection of either homologously recombined bacterial artificial chromosomes (BACs) (Tallini, Shui, et al., 2006), or previously established promoter constructs with desired effector or reporter, into fertilized single cell eggs. All constructs are listed in Table 1. The optogenetic effector lines contained either optoα1AR (Airan et al., 2009), optoß2AR (Airan et al., 2009), or CatCh2 (Zhang et al., 2006) genes linked to downstream IRES-lacZ for simple identification of transgene expression. The reporter lines contained either EGFP- or RFP-derived GECIs as single fluorophores (GCaMP8/8.1 or RCaMP1.07) or a fusion protein of green and red fluorophores (GCaMP8.1-mVermilion or GCaMP5-mCherry). BAC transgenes were constructed by homologous recombination to position the desired transgene in frame with the initiation codon of the native gene as previously described (Tallini, Shui, et al., 2006). Purified BAC transgene plasmids were microinjected into single-cell embryos at the Cornell University Transgenic Core Facility or the UC Irvine Transgenic Mouse

Facility. Pups were screened for the desired transgene by PCR analysis using primers listed in Online Table I, backcrossed to C57BL/6J and further screened by immunohistochemistry, X-gal staining, or fluorescence imaging using standard methods. Briefly, tissues were either fixed overnight in 4% paraformaldehyde (PFA) at 2-8°C, rinsed in 1x phosphate-buffered saline (PBS) and equilibrated in 30% sucrose/1x PBS at 2-8°C (for immunohistochemistry), or fixed for 2 hrs in 4% PFA on ice (for X-gal staining, see Appendix) and processed to 30% sucrose. Anti-GFP or anti-dsRed antibodies were used as previously described (Jesty et al., 2012). For fluorescence imaging, sections were washed three times in 1X PBS, mounted with VectaShield with DAPI (Vector Laboratories), and imaged using a Leica DMI6000B inverted microscope. Monochrome images were colorized using ImageJ software (Appendix).

Ex-vivo arterial imaging

Freshly isolated mid cerebral or mesenteric arteries were cannulated on glass pipettes mounted in a 5 mL myograph chamber and pressurized as described previously (Prada et al., 2019), and only arteries that constricted more than 30% to isosmotic physiological salt solution containing 120 mM KCl were used. Optogenetic effector proteins were activated at 473 nm using in an Olympus FV1000 microscope with a SIM scanner, which enables photostimulation. To avoid unintended activation of genetic proteins by ambient light, the isolated vessels were kept in the dark or under red light. Arterial diameter was determined from stacks of tiff images using the Myotracker video-edge detection plugin in ImageJ (Fernandez, Bankhead, Zhou, McGeown, & Curtis, 2014).

Ex vivo heart imaging

Mice were given 100U of heparin IV immediately prior to euthanasia by pentobarbital (120 mg/kg, IP). The heart was quickly excised with aorta and vena cava vessels attached and rinsed in ice cold Tyrode's buffer (137mM NaCl; 2.7mM KCl; 10mM HEPES; 1.4mM $CaCl_2$; 1.0mM $MgCl_2$; 0.4mM NaH_3PO_4; 12mM $NaHCO_3$; 5.5mM D-glucose; pH 7.4). The rinsed heart was cannulated and perfused with warm Tyrode's buffer (37°C, equilibrated with 95% O_2/5% CO_2). GCaMP8 fluorescence was captured using an Andor-iXon CCD camera mounted on an Olympus MVX10 fluorescent microscope (ex: 472/30 nm, em: 520/35 nm).

In vivo heart stimulation

Mice were anesthetized with ketamine (100 mg/kg) and xylazine (10 mg/kg) via intraperitoneal injection, intubated with a 22-gauge cannula, ventilated (95 breath/min, 12 cm H_2O end-inspiratory pressure; CWE SAR-830/P ventilator), and maintained on 1.5% isoflurane. 5% glucose (0.1 mL/10 g) and atropine sulfate (5 µg/100 g body weight) were injected subcutaneously and body temperature was maintained at 37.5°C with a heating pad. The heart was surgically exposed by dissection of the sternum and diaphragm, and ribs retracted for optical access to the thoracic cavity. For optical stimulation of the SA-node, mice were positioned on their back on a stereotaxic stage, the pericardial sac was removed, and the thymus gland repositioned from covering the right atrium. Illumination of the node was performed using a 105-µm core fiber (Thorlabs) coupled to a 473-nm continuous wave, diode-pumped solid-state laser system (Opto Engine LLC; BL-473-00200-CWM-SD-03-LED-F). The tip of the laser fiber was inserted through 500-µm metal tubing and clamped within a four-way axis

micromanipulator that allowed positioning of the fiber tip on the anterior junction of the right atrium and superior vena cava. For stimulation of the left ventricle free wall, mice were positioned on their right side and a left thoracotomy was performed between ribs 7 – 8 to gain access to the heart. The tip of the optical fiber was coupled to a collimating lens mount that was positioned to direct the beam at the left ventricle. A customized titanium probe affixed to the stereotaxic stage was adhered (Vetbond) to the left ventricle free wall to minimize movement associated with respiratory and cardiac contractions. Electrocardiogram (ECG) electrodes were attached to 21-gauge needles inserted subcutaneously through the front and contralateral hind limb and recorded with an isolated differential amplifier (World Precision Instruments; #ISO-80). ECG and lung pressure traces were continuously monitored through an oscilloscope. Laser pulses were controlled through a TTL signal delivered by a function generator (Agilent 33210A) and signals digitized and recorded on a computer using MATLAB.

SA node stimulation

For *in vivo* stimulation of the SA nodal tissue, the mouse was anesthetized with 1.5% isoflurane and positively ventilated by intubation as described above. The ECG electrodes were attached and the heart was visualized by opening the thoracic cavity. The metal tube containing the fiber optic cable was placed adjacent to the SA node. The laser was controlled as described above and the ECG recorded. For *ex vivo* stimulation, the fiber optic cable was positioned over the SA nodal tissue of the excised heart and laser controlled as described above.

In vivo 2-photon imaging

A left thoracotomy was performed as above and a 3D-printed titanium stabilization probe with imaging window (Allan-Rahill, Lamont, Chilian, Nishimura, & Small, 2020; Jones, Small, & Nishimura, 2018) attached to the left ventricle free-wall using tissue adhesive (Vetbond). Texas-Red conjugated 70-kDa dextran (3% in saline; Thermo Fischer Scientific #D1830) was injected retro-orbitally to identify the vasculature. A Ti:Sapphire laser (Chameleon, Coherent) with wavelength centered at 950 nm was used to excite indicator molecules and images collected using a custom multiphoton microscope equipped with four detection channels and high-speed resonant scanners running ScanImage (Pologruto, Sabatini, & Svoboda, 2003). Emission fluorescence was detected using long-pass dichroic mirrors and bandpass filters for GCaMP8 (517/65 nm) and Texas-Red (629/56). Water was placed within a rubber O-ring of the stabilization probe to allow immersion of the microscope objective (Olympus XLPlan N 25x 1.05 NA). ECG and respiratory signals were collected while imaging z-stacks (50-100 frames; 2 μm per z-step; 30 frames/sec) in 4 – 5 different regions in each mouse. Image reconstruction was performed as previously described(Jones et al., 2018), by indexing image lines based on their acquired position within the cardiac or respiratory cycles. Additional analysis is described in Supplemental Materials.

In vivo arterial imaging

Mice were anesthetized with 5% isoflurane, maintained with 2% isoflurane using a nose cone, and placed on a heated stage. The cremaster or femoral vessels were visualized and superfused with warm PSS equilibrated with 95% O_2-5% CO_2 (Bagher & Segal, 2011). Endothelial cells of either cremaster or femoral vessels were stimulated with a

473-nm, continuous wave, diode-pumped solid-state laser system (Opto Engine LLC; BL-473-00200-CWM-SD-03-LED-F) at power and pulse length as specified. Optical fiber coupled to a collimating lens was attached to a 3-axis micromanipulator and positioned to aim the light at the desired vessel. To quantify arterial diameter changes, vessels were illuminated with white light. Raw images from the Andor-iXon camera were converted to tif files using ImageJ. Motion artefacts between frames were removed using MATLAB's Image Processing Toolbox prior to vessel analysis. Each frame was translated to maximize the 2-dimensional correlation with respect to the first frame using the function *imregcorr*. This correlation was calculated in an area of the images not affected by light leakage from the stimulation laser in order to avoid stabilizing on the beam rather than the tissue structure. Once the image was stabilized, vessel width and sidewall intensity were measured as a function of time across each frame. MATLAB was used to interpolate the intensity profile along a user-specified line across a vessel using the *interp2* function. To improve the resulting profile, intensity was averaged over 28.05 μm. The two peaks in the profile were recorded as the sidewall intensities and the distance between the peaks recorded as the vessel width. If the profile still included significant noise, a quadratic fit was performed around each peak to find a more accurate peak location and intensity.

ECG analysis

ECG and laser pulse recordings were loaded into MATLAB. Appropriate pre-processing was performed to (1) (when necessary) re-sample non-continuous recordings, (2) lowpass filter ECGs with a passband frequency of 100 Hz, (3) invert, scale, and shift ECGs to have a median value of zero and a maximum amplitude of one, and (4)

binarize laser pulse recordings. ECG R-wave peaks were detected automatically using MATLAB's *findpeaks* function, and P-waves were detected by finding the local maximum within a ~100 ms window before the R-wave. All peaks were manually curated and adjusted as necessary. Beats were classified as unstimulated if they occurred before the onset of stimulation pulses. For αMHC-CatCh2 recordings**,** beats were classified as stimulated if an R-wave occurred 10-38 ms after a laser pulse rising edge, and for HCN^{BAC}-CatCh2 recordings, beats were classified as stimulated if a P-wave occurred 38-52 ms after a laser pulse falling edge. Beats occurring after onset of stimulation but that did not meet the timing criteria were excluded from analysis. R-wave duration was calculated as the time interval between zero-crossings on either side of the R-wave. PR interval was calculated as the time interval between peak P-wave and the first zero crossing of the QRS complex. PR intervals and R-wave durations were imported into prism to generate violin plots and calculate p-values using the Mann-Whitney Test.

MATLAB data transformation and statistical analysis

The raw data for vessel width from MATLAB analysis was transformed using the running average algorithm in SigmaPlot 11 and the transformed data was copied to Excel spreadsheet. The net change in vessel width was calculated by finding the minimum width in the first 10 seconds after laser activation using the MIN function in Microsoft Excel and subtracting this value from SigmaPlot transformed data.

The % change in vessel width was calculated by first determining the maximum width during laser activation using the MAX function in Microsoft Excel and using the formula ((MAX – MIN)/MIN)*100. The % change in vessel width from 3 femoral vessels from

Cdh5^{BAC}-Optoα1AR and C57BL/6J animals were determined and compared using the Holm-Sedak method (SigmaPlot v 11).

Patch-Clamp Electrophysiology

All current recordings were acquired at room temperature using an Axopatch200B amplifier and a Digidata1440 digitizer (Molecular Devices, Sunnyvale, CA). Borosilicate patch pipettes were pulled and polished to resistance of 3-6 MΩ for all experiments using a micropipette puller (model P-97, Sutter Instruments, Novato, CA). Freshly dissociated arterial myocytes were kept in ice-cold Mg^{2+}-PSS before being recorded.

Voltage-gated K^+ (I_K) and light-activated CatCh2 (I_{Cat}) currents were recorded using conventional whole-cell configuration of the voltage-clamp technique. Currents were recorded at a frequency of 50 kHz and low-pass filtered at 2 kHz. I_K and I_{Cat} were recorded while cells were exposed to an external solution composed of 130 mM NaCl, 5 mM KCl, 3 mM $MgCl_2$, 10 mM Glucose, and 10 mM HEPES adjusted to 7.4 using NaOH. The pipette solution was composed of 87 mM K-Aspartate, 20 mM KCl, 1 mM $CaCl_2$, 1 mM $MgCl_2$, 5 mM MgATP, 10 mM EGTA, and 10 mM HEPES adjusted to 7.2 by KOH. A liquid junction potential of 12.7 mV was corrected offline. I_K were activated by a series of 500 ms test pulses increasing from -70 mV to +60 mV. I_{Cat} was recorded while cells were held at -70 mV before and after exposure to 488 nm light.

Acknowledgements

We thank the Cornell Stem Cell and Transgenics Core, and the University of California, Irvine Transgenic Mouse Facility (TMF) for production of BAC transgenic mice. The UCI TMF is a shared resource funded in part by the Chao Family Comprehensive Cancer Center Support Grant (P30CA062203) from the National Cancer Institute.

Sources of Funding

This work was supported by NIH R24 HL120847 to M.I.K, AHA 13SDG17330004 and NIH P01AI102851 and R21 AG058173 to N.N, R01 HL122827 to M.A.R., R01 HL121059 and R01 HL149127 to M.F.N, and R01 HL152681and OT2 OD026580 to L.F.S. D.M.S was supported by AHA fellowship 17POST3368012.

Disclosures

Authors declare no conflict of interests.

References

Airan, R. D., Thompson, K. R., Fenno, L. E., Bernstein, H., & Deisseroth, K. (2009). Temporally precise in vivo control of intracellular signalling. *Nature, 458*(7241), 1025-1029.

Akerboom, J., Carreras Calderon, N., Tian, L., Wabnig, S., Prigge, M., Tolo, J., . . . Looger, L. L. (2013). Genetically encoded calcium indicators for multi-color neural activity imaging and combination with optogenetics. *Front Mol Neurosci, 6*, 2. doi:10.3389/fnmol.2013.00002

Allan-Rahill, N. H., Lamont, M. R. E., Chilian, W. M., Nishimura, N., & Small, D. M. (2020). Intravital microscopy of the beating murine heart to understand cardiac leukocyte dynamics. *Front Immunol, 11*, 92. doi:10.3389/fimmu.2020.00092

Asimaki, A., Kleber, A. G., MacRae, C. A., & Saffitz, J. E. (2014). Arrhythmogenic cardiomyopathy - new insights into disease mechanisms and drug discovery. *Prog Pediatr Cardiol, 37*(1-2), 3-7. doi:10.1016/j.ppedcard.2014.10.001

Bagher, P., & Segal, S. S. (2011). The mouse cremaster muscle preparation for intravital imaging of the microcirculation. *J Vis Exp*(52). doi:10.3791/2874

Bethge, P., Carta, S., Lorenzo, D. A., Egolf, L., Goniotaki, D., Madisen, L., . . . Helmchen, F. (2017). An r-camp1.07 reporter mouse for cell-type-specific expression of a sensitive red fluorescent calcium indicator. *PLoS One, 12*(6), e0179460. doi:10.1371/journal.pone.0179460

Bui, A. L., Horwich, T. B., & Fonarow, G. C. (2011). Epidemiology and risk profile of heart failure. *Nat Rev Cardiol, 8*(1), 30-41. doi:10.1038/nrcardio.2010.165

Delorme, B., Dahl, E., Jarry-Guichard, T., Marics, I., Briand, J. P., Willecke, K., . . . Theveniau-Ruissy, M. (1995). Developmental regulation of connexin 40 gene expression in mouse heart correlates with the differentiation of the conduction system. *Dev Dyn, 204*(4), 358-371. doi:10.1002/aja.1002040403

DiFrancesco, D. (1993). Pacemaker mechanisms in cardiac tissue. *Annu Rev Physiol, 55*, 455-472. doi:10.1146/annurev.ph.55.030193.002323

Duncker, D. J., & Bache, R. J. (2008). Regulation of coronary blood flow during exercise. *Physiol Rev, 88*(3), 1009-1086. doi:10.1152/physrev.00045.2006

Fenno, L., Yizhar, O., & Deisseroth, K. (2011). The development and application of optogenetics. *Annu.Rev.Neurosci., 34*, 389-412.

Fernandez, J. A., Bankhead, P., Zhou, H., McGeown, J. G., & Curtis, T. M. (2014). Automated detection and measurement of isolated retinal arterioles by a combination of edge enhancement and cost analysis. *PLoS One, 9*(3), e91791. doi:10.1371/journal.pone.0091791

Gengyo-Ando, K., Kagawa-Nagamura, Y., Ohkura, M., Fei, X., Chen, M., Hashimoto, K., & Nakai, J. (2017). A new platform for long-term tracking and recording of neural activity and simultaneous optogenetic control in freely behaving caenorhabditis elegans. *J Neurosci Methods, 286*, 56-68. doi:10.1016/j.jneumeth.2017.05.017

Gonzales, A. L., Klug, N. R., Moshkforoush, A., Lee, J. C., Lee, F. K., Shui, B., . . . Nelson, M. T. (2020). Contractile pericytes determine the direction of blood flow at capillary junctions. *Proc Natl Acad Sci U S A, 117*(43), 27022-27033. doi:10.1073/pnas.1922755117

Gonzalez-Lopez, E., & Vrana, K. E. (2020). Dopamine beta-hydroxylase and its genetic variants in human health and disease. *J Neurochem, 152*(2), 157-181. doi:10.1111/jnc.14893

Gulick, J., Subramaniam, A., Neumann, J., & Robbins, J. (1991). Isolation and characterization of the mouse cardiac myosin heavy chain genes. *J Biol Chem, 266*(14), 9180-9185.

Jesty, S. A., Steffey, M. A., Lee, F. K., Breitbach, M., Hesse, M., Reining, S., . . . Kotlikoff, M. I. (2012). C-kit+ precursors support postinfarction myogenesis in the neonatal, but not adult, heart. *Proc.Natl.Acad.Sci.U.S.A*.

Johnson, R. P., El-Yazbi, A. F., Hughes, M. F., Schriemer, D. C., Walsh, E. J., Walsh, M. P., & Cole, W. C. (2009). Identification and functional characterization of protein kinase a-catalyzed phosphorylation of potassium channel kv1.2 at serine 449. *J Biol Chem, 284*(24), 16562-16574. doi:10.1074/jbc.M109.010918

Jones, J. S., Small, D. M., & Nishimura, N. (2018). In vivo calcium imaging of cardiomyocytes in the beating mouse heart with multiphoton microscopy. *Front Physiol, 9*, 969. doi:10.3389/fphys.2018.00969

Joyner, A., & Wall, N. (2008). Immunohistochemistry of whole-mount mouse embryos. *CSH Protoc, 2008*, pdb prot4820. doi:10.1101/pdb.prot4820

Kotlikoff, M. I. (2007). Genetically encoded ca2+ indicators: Using genetics and molecular design to understand complex physiology. *J Physiol, 578*(Pt 1), 55-67.

Luykenaar, K. D., & Welsh, D. G. (2007). Activators of the pka and pkg pathways attenuate rhoa-mediated suppression of the kdr current in cerebral arteries. *Am J Physiol Heart Circ Physiol, 292*(6), H2654-2663. doi:10.1152/ajpheart.01255.2006

Mack, C. P., & Owens, G. K. (1999). Regulation of smooth muscle alpha-actin expression in vivo is dependent on carg elements within the 5' and first intron promoter regions. *Circ Res, 84*(7), 852-861. doi:10.1161/01.res.84.7.852

Madisen, L., Zwingman, T. A., Sunkin, S. M., Oh, S. W., Zariwala, H. A., Gu, H., . . . Zeng, H. (2010). A robust and high-throughput cre reporting and characterization system for the whole mouse brain. *Nat Neurosci, 13*(1), 133-140. doi:10.1038/nn.2467

Meyers, J. D., Jay, P. Y., & Rentschler, S. (2016). Reprogramming the conduction system: Onward toward a biological pacemaker. *Trends Cardiovasc Med, 26*(1), 14-20. doi:10.1016/j.tcm.2015.03.015

Mond, H. G., & Proclemer, A. (2011). The 11th world survey of cardiac pacing and implantable cardioverter-defibrillators: Calendar year 2009--a world society of arrhythmia's project. *Pacing Clin Electrophysiol, 34*(8), 1013-1027. doi:10.1111/j.1540-8159.2011.03150.x

Moosmang, S., Stieber, J., Zong, X., Biel, M., Hofmann, F., & Ludwig, A. (2001). Cellular expression and functional characterization of four hyperpolarization-activated pacemaker channels in cardiac and neuronal tissues. *Eur J Biochem, 268*(6), 1646-1652. doi:10.1046/j.1432-1327.2001.02036.x

Nakai, J., & Ohkura, M. (2003). Probing calcium ions with biosensors. *Biotechnol Genet Eng Rev, 20*, 3-21. doi:10.1080/02648725.2003.10648035

Nakamura, K., & Murry, C. E. (2019). Function follows form- a review of cardiac cell therapy. *Circ J, 83*(12), 2399-2412. doi:10.1253/circj.CJ-19-0567

Nelson, M. T., & Quayle, J. M. (1995). Physiological roles and properties of potassium channels in arterial smooth muscle. *Am J Physiol, 268*(4 Pt 1), C799-822. doi:10.1152/ajpcell.1995.268.4.C799

Nyns, E. C. A., Poelma, R. H., Volkers, L., Plomp, J. J., Bart, C. I., Kip, A. M., . . . Pijnappels, D. A. (2019). An automated hybrid bioelectronic system for autogenous restoration of sinus rhythm in atrial fibrillation. *Sci Transl Med, 11*(481). doi:10.1126/scitranslmed.aau6447

Ohkura, M., Sasaki, T., Sadakari, J., Gengyo-Ando, K., Kagawa-Nagamura, Y., Kobayashi, C., . . . Nakai, J. (2012). Genetically encoded green fluorescent ca2+ indicators with improved detectability for neuronal ca2+ signals. *PLoS One, 7*(12), e51286. doi:10.1371/journal.pone.0051286

Pologruto, T. A., Sabatini, B. L., & Svoboda, K. (2003). Scanimage: Flexible software for operating laser scanning microscopes. *Biomed Eng Online, 2*, 13. doi:10.1186/1475-925X-2-13

Prada, M. P., Syed, A. U., Buonarati, O. R., Reddy, G. R., Nystoriak, M. A., Ghosh, D., . . . Navedo, M. F. (2019). A gs-coupled purinergic receptor boosts ca(2+) influx and vascular contractility during diabetic hyperglycemia. *Elife, 8*. doi:10.7554/eLife.42214

Sonkusare, S. K., Bonev, A. D., Ledoux, J., Liedtke, W., Kotlikoff, M. I., Heppner, T. J., . . . Nelson, M. T. (2012). Elementary ca2+ signals through endothelial trpv4 channels regulate vascular function. *Science, 336*(6081), 597-601. doi:10.1126/science.1216283

Sonkusare, S. K., Dalsgaard, T., Bonev, A. D., Hill-Eubanks, D. C., Kotlikoff, M. I., Scott, J. D., . . . Nelson, M. T. (2014). Akap150-dependent cooperative trpv4 channel gating is central to endothelium-dependent vasodilation and is disrupted in hypertension. *Sci Signal, 7*(333), ra66. doi:10.1126/scisignal.2005052

Straub, A. C., Zeigler, A. C., & Isakson, B. E. (2014). The myoendothelial junction: Connections that deliver the message. *Physiology (Bethesda), 29*(4), 242-249. doi:10.1152/physiol.00042.2013

Tallini, Y. N., Brekke, J. F., Shui, B., Doran, R., Hwang, S. M., Nakai, J., . . . Kotlikoff, M. I. (2007). Propagated endothelial ca2+ waves and arteriolar dilation in vivo: Measurements in cx40bac gcamp2 transgenic mice. *Circ Res, 101*(12), 1300-1309. doi:10.1161/CIRCRESAHA.107.149484

Tallini, Y. N., Ohkura, M., Choi, B. R., Ji, G., Imoto, K., Doran, R., . . . Kotlikoff, M. I. (2006). Imaging cellular signals in the heart in vivo: Cardiac expression of the high-signal ca2+ indicator gcamp2. *Proc Natl Acad Sci U S A, 103*(12), 4753-4758. doi:10.1073/pnas.0509378103

Tallini, Y. N., Shui, B., Greene, K. S., Deng, K. Y., Doran, R., Fisher, P. J., . . . Kotlikoff, M. I. (2006). Bac transgenic mice express enhanced green fluorescent protein in central and peripheral cholinergic neurons. *Physiol Genomics, 27*(3), 391-397.

Tian, L., Hires, S. A., Mao, T., Huber, D., Chiappe, M. E., Chalasani, S. H., . . . Looger, L. L. (2009). Imaging neural activity in worms, flies and mice with improved gcamp calcium indicators. *Nat Methods, 6*(12), 875-881. doi:10.1038/nmeth.1398

Tsien, R. Y. (2003). Breeding molecules to spy on cells. *Harvey Lect., 99*, 77-93.

Vedantham, V. (2015). New approaches to biological pacemakers: Links to sinoatrial node development. *Trends Mol Med, 21*(12), 749-761. doi:10.1016/j.molmed.2015.10.002

Wellman, G. C., Santana, L. F., Bonev, A. D., & Nelson, M. T. (2001). Role of phospholamban in the modulation of arterial ca(2+) sparks and ca(2+)-activated k(+) channels by camp. *Am J Physiol Cell Physiol, 281*(3), C1029-1037. doi:10.1152/ajpcell.2001.281.3.C1029

Welsh, D. G., & Segal, S. S. (1998). Endothelial and smooth muscle cell conduction in arterioles controlling blood flow. *Am J Physiol, 274*(1 Pt 2), H178-186.

Zariwala, H. A., Borghuis, B. G., Hoogland, T. M., Madisen, L., Tian, L., De Zeeuw, C. I., . . . Chen, T. W. (2012). A cre-dependent gcamp3 reporter mouse for neuronal imaging in vivo. *J.Neurosci., 32*(9), 3131-3141.

Zhang, F., Wang, L. P., Boyden, E. S., & Deisseroth, K. (2006). Channelrhodopsin-2 and optical control of excitable cells. *Nat.Methods, 3*(10), 785-792.